Human Head FE Modeling: Improvement of Skull Geometry and Brain Constitutive Laws

C. Deck, S. Nicolle, R. Willinger

Strasbourg University, ULP-IMFS-CNRS 7507, 2 rue Boussingault 67000 Strasbourg, France.

Abstract −Traumatic head injuries remain a common cause of death and severe disabilities around the world. FE modeling of the head is a well accepted tool to study head impact biomechanics. This paper investigates improvements to a number of geometrical aspects and material constitutive laws of this complex human segment. The objective of the present study is to improve both, the skull and brain modeling. The skull representation is improved at the geometrical point of view in order to simulate skull depressive and linear fractures. At the other hand brain constitutive law improvement is based on original experimental tests focusing on high strain rates and non linear behavior in order to investigate the brain material properties influence in the head model validation procedure against existing experimental brain deformation recording. Main result is a detailed skull geometry including skull reinforced beams and thickness variation validated against existing head impacts involving skull fracture as well as a linear and a non-linear brain constitutive law which permit an accurate validation against brain deformation under impact.

Keywords : Biomechanics, Head FE model, Skull reinforced beams, Brain laws.

1 Introduction

Traumatic Head Injury remain a common cause of death and severe disabilities around the world. If FE modeling of the head is a well accepted tool for head impact biomechanics research a number of geometrical aspects and material constitutive laws of this complex human segment need further developments. Over the past few years, 3D Finite Element Models of the human head have been powerful tools used to understand and to predict the head's response under impact conditions.

The first tentative proposals for injury criteria was made by Willinger et al. (2000 and 2003) who simulated 64 accidents reconstructions using the ULP FE model. The concussion was correlated with intra-cerebral Von Mises stress of about 20 kPa, strain energy in the CSF layer of 4J was proposed as a threshold for sub-dural haematoma and a Tsaï-Wu criterion was suggested for the prediction skull fracture. King et al. in 2003, in reproducing 53 accident cases with the WSU model (Zhang et al., 2001), shows that strain rate and the product of strain and strain rate in the midbrain region appeared to be the best injury predictors for concussion. More recently, Takhounts et al.(2003) using SIMon FE model propose three injury metrics : cumulative strain damage measure for diffuse axonal injury, dilatational damage measure to estimate the potential for contusions, and relative motion damage measure for acute subdural hematoma.

Existing FE models describe in detail the complex geometry but none of them include the reinforced beams of the skull. These skull reinforcement structures are supposed to play and important role in its dynamical response to impact so it is an important safety aspect as far as pedestrian safety is concerned.

The second shortcoming of existing models is the lack of data on constitutive law of brain tissue in finite deformation and in very short times corresponding with traffic accidents. Indeed, brain injuries can be associated to the large strains during which the brain's tolerance threshold is exceeded and the cerebral tissue is torn (Thibault et al., 1990). This dynamic process is more and more addressed in recent literature (Bilston et al., 2001; Brands et al., 2000; Darvish et al., 2001; Donnelly et al., 1997; Mendis et al., 1995; Prange et al., 2000). Moreover, typical frequency content of the impact spectrum during direct head impact are of the order of 1000 Hz (Hickling et al., 1973; Peters et al., 1997), i.e. corresponds with very short acceleration's peak but, until now, no direct experimental result is available in this relevant dynamic range in the literature. Dynamical behaviour of the brain is a great relevance to assess the risks of traumatic brain injury under impact loading. However, no result is available in the literature on the mechanical properties of the brain in shear corresponding to both relevant frequency ranges of accidental

(300-1000Hz)and ballistic direct impacts (1000-3000Hz).

Finally, a great discrepancy (in amplitude and frequency-dependence of the shear moduli) in the linear field can be observed in the literature's results due to interspecies and testing protocol differences. In addition, only the elastic part of the brain's behaviour is often taken into account in the Finite Element Models of the head because the model's parameters are calculated from the relaxation modulus deduced from the only storage modulus by approximate Christensen's equation (Christensen, 1982). It is well-known that the modelling of only one part (the elastic in this case) of the material's behaviour leads to a multiple set of parameters which do not suit necessarily the second part of the behaviour. The consequences may be important under impact conditions when the viscous part is badly estimated.

Globally, more than 30 years of research on the mechanical properties of the brain tissue have been motivated by traumatic injury prevention. In most of these studies it is assumed that the brain tissue is incompressible (McElhaney et al., 1976; Stalnaker, 1969) and is therefore most likely to fail in shear. It is the reason why the results are usually presented in terms of frequency-dependant complex shear moduli. For ethical and technical reasons, these studies are performed on in vitro brain tissue. Fallenstein et al. (1969) measured the storage (G') and the loss (G'') modulus of human brain at 10 Hz and found that G' and G'' lie between 0.6 and 1.10 kPa and 0.35 and 0.60 kPa respectively. The applied strain levels varied from 7% to 24.5% in this study. Shuck et al. (1972) reported the complex shear moduli of human brain tissue between 5 and 350 Hz ranging from 7.6 to 39.4 kPa for G' and from 2.8 to 81.4 kPa for G'' and noted brain damages beyond 1.3% of strain. They proposed a linear four-parameter-fluid model to fit the results at the higher frequencies but this model was not satisfactory below 100 Hz. Bilston et al. (1997) performed shear relaxation and oscillatory experiments on bovine brain tissue. These authors determined a linear viscoelastic strain limit of the order of 0.1% and suggested that brain tissue had a fluid-like behaviour since shear relaxation data did not indicate the presence of a long-term elastic modulus. The scopes of the dynamic shear moduli were found to be extended from 1 to 5 kPa and from 0.5 to 0.4 kPa for G' and G" respectively between 0.005 and 20 Hz. Peters et al. (1997) applied the time/temperature superposition principle to brain tissue. They calculated a dynamic shear modulus ranging from 0.3 kPa to 10 kPa between 0.1 and 10^6 Hz for the porcine brain tissue. Brands et al. (2002) applied this principle to determine a linear multi-mode Maxwell model from small strain oscillatory experiments on the porcine brain tissue. The extrapolated storage (G') and loss (G'') moduli lie between 0.5 and 1.8 kPa and 0.2 and 1.5 kPa respectively for a frequency ranging from 0.16 to 1000 Hz. Finally, Arbogast et al. (1997) measured the complex shear moduli of the porcine brain tissue and found G' ranging from 1.25 to 1.65 kPa and G'' ranging from 0.4 to 2.15 kPa as frequency increased from 20 to 200 Hz. In these experiments, the applied strains were either 2.5% to 5%. A synthesis of these experimental approaches is illustrated in Figure 6, where results of the present study are exposed. Main limitations of existing results besides the large discrepancy is the restricted frequency range and the shortcoming in the modelling of both elastic and viscous behaviours. Non linear brain material has also been investigated (Brands et al., 2002, Kleiven et al., 2002). These first experimental attempts and modelling of brain behaviour under large strain needs further analysis and validation.

This study presents an improved head FE model with a detailed skull geometry including thickness variation and the anatomical reinforced beams. Model improvement concerns also brain material simulation based on new experimental investigation in the linear and non-linear domain.

For the model validation process head impact from the literature involving fracture were simulated. Then, new linear and non-linear brain's constitutive model were implemented in an explicit FE code (Radioss) in order to investigate the influence of brain mechanical properties on brain deformation under head impact simulation. This point was conducted accordingly to Hardy's experimental head impact data focussing on brain deformation recording (Hardy et al.,2001).

2 Skull Modeling Improvement

The new head model is based on the geometry of Strasbourg ULP finite element head model (Kang et al., 1997). Skull geometry is obtained by a 3D digitising of the outer and inner surface of a 50th

percentile human adult male skull (Figure 1a). Figure 1b shows the 3D-skull surface obtained by digitising external and internal surfaces of the skull. Special attention is paid to the evolution of skull thickness throughout the skull. As a consequence the diploë is meshed by 3D brick elements. Outer and inner tables are represented by constant thickness shell elements (1mm). A special attention was paid to the quality of the meshing. Indeed, during its creation, it is extremely significant to consider the time step of computing which would be imposed by small sizes or distorted elements. In the computer code used (Radioss), the time step of computing is given according to the size of the elements, the state of deformation and the mechanical properties. The average characteristic length of the brick and shell elements was around 2 and 2.5mm respectively.

In addition, the anatomical reinforced beams are integrated in this new skull meshing according to the Kamina anatomic atlas (2002) as illustrated in the Figure 2a.

With regard to the outer table we differentiated the frontal beam (Crista frontalis), the zigomatic arch (Arcus zygomaticus), the spheno-frontal beam (Ala minor ossis sphenoidalis), the lateral superior and inferior arches (Linea temporalis superior, inferior), the semi-circular occipital arch (Sulcus sinus transversi) and the mastoïdian pilar (Processus mastoideus).

For the inner table, we took into account the spheno-frontal beam (Ala minor ossis sphenoidalis), the sphenoïdal arch (arcus sphenoidalis), the occipital beam, the petrouse beam (Sulcus sinus sigmoidei) and the occipital beam (Crista occipitalis interna) as shown in Figure 2b and 2c.

The skull geometry is characterised by the integration of these 14 reinforced beams, its thickness variation by a meshing of the diploe with brick elements.

The detailed skull model is build of 25496 shell elements for the inner and outer table and 16 322 brick elements for the diploë.

This meshing is not continuous between the outer table and the diploë and between the diploë and the inner table, so two tied contact interfaces were implemented.

Material characteristics are very important to the success of a finite element model. An elastic-plastic Johnson cook material model was used for cortical and cancellous bones. This law models the material as linear elastic but when the yield stress is reached, the material behaves plastically. Equation 1 describes the stress evolution during plastic deformation.

$$\sigma = \left(a + b\varepsilon_p^n\right)\left(1 + c\ln\frac{\dot{\varepsilon}}{\dot{\varepsilon}0}\right) \qquad (1)$$

With “a” the yield stress, “b” the hardening modulus, “n” the hardening exponent, “c” the strain rate coefficient and “” the reference strain rate.

Damage elements available in the Radioss material model was used to predict bone fractures. Elements rupture occurs if the plastic strain is larger than a maximum stress. If the element is a shell the failed element is deleted and if the element is a solid element it has its deviatoric stress tensor permanently set to zero.

Material properties related to the improved skull come from McElhaney (1973) and Wood (1971), and are reported in Table 1.

To take into account the reinforced beams, we doubled the thickness of the shell cortical bone. For the inner table, the spheno-frontal beam, the sphenoïdal arch, the occipital beam, the petrouse beam and the occipital beam is defined with a 2mm shell thickness. Concerning the outer table a thickness of 2mm is applied to distinguish the frontal beam, the zigomatic arch, the spheno-frontal beam, the lateral superior and inferior arches, the semi-circular occipital arch and the mastoïdian pilar.

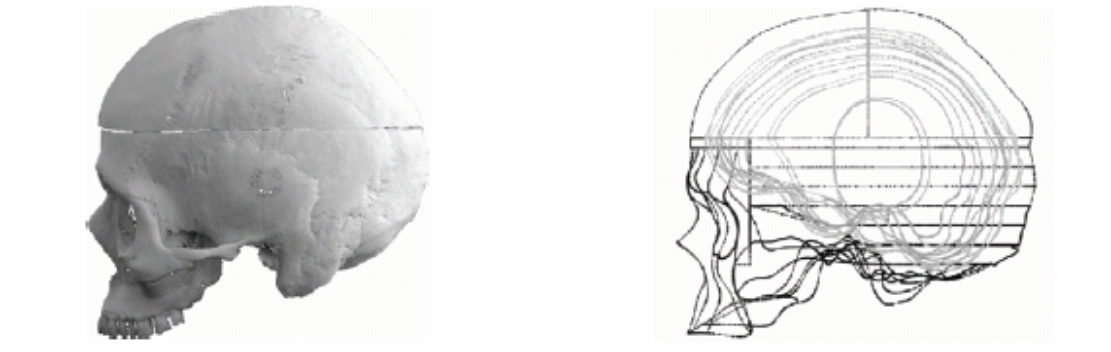

(a) (b)

Fig.1 (a) dry human adult skull and (b) 3D inner and outer surfaces caption.

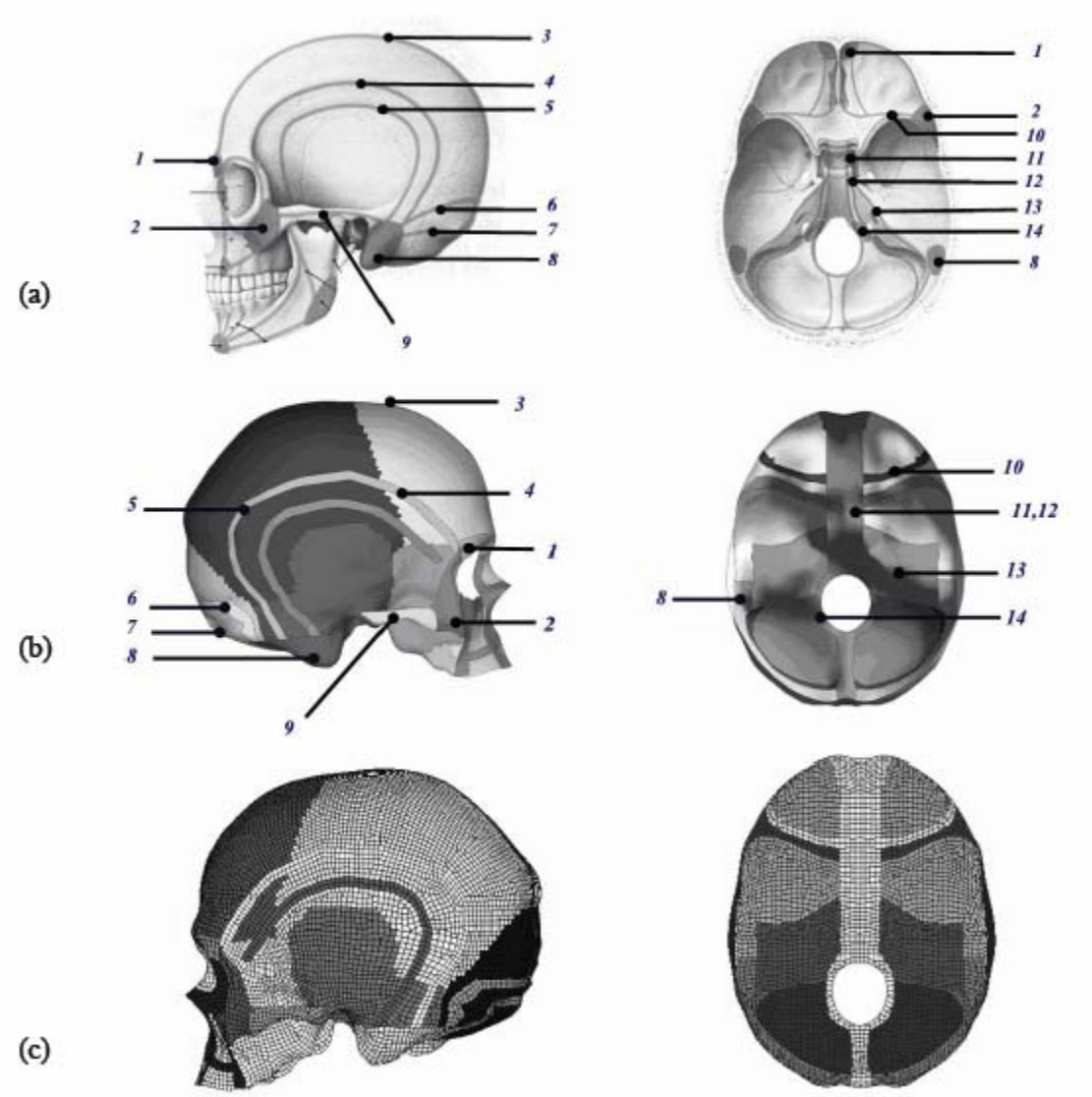

Fig. 2 (a)Location of the reinforced beams, (b) outer and inner surfaces, (c)the meshing

1. Frontal beam, 2. Zigomatic arch, 3. Spheno-frontal beam, 4.5. Lateral superior and inferior arches, 6.7. Semi-circular occipital arch, 8. Mastoïdian pilar, 9. Zigomatic arch, 10. Spheno-frontal beam, 11. Sphenoïdal arch, 12. Occipital beam, 13. Petrouse beam, 14. Occipital beam.

Table 1 Material properties of the human skull FE model

Part	Material property	Material parameter	Value	Element type	Shell thickness
Cranium (Cortical)	Elastic-plastic with damage	Density	1900 Kg.m^{-3}	Shell	1 mm (skull) 2 mm (reinforced beams)
		Young modulus	12200 MPa		
		Poisson's ratio	0.21		
		Yield stress (a)	90 MPa		
		Hardening modulus (b)	0.1		
		Hardening exponent (n)	0.1		
		Failure strain	0.2E-03		
Cranium (Trabecular)	Elastic-plastic with damage	Density	1500 Kg.m^{-3}	Solid	-----
		Young modulus	1000 MPa		
		Poisson's ratio	0.05		
		Yield stress (a)	28 MPa		
		Hardening modulus (b)	0.1		
		Hardening exponent (n)	0.1		
		Failure strain	0.1E-03		

3 Experimental Brain Characterisation

Porcine brain tissue was harvested from two six-months-old pigs obtained from a local slaughterhouse. Immediately after death, the complete brains were preserved in a Ringer-Lactate solution to prevent dehydration. In the present study, less than 6% of change in the shear properties of brain tissue was observed from samples tested at 24-hour interval. A similar conclusion was given by McElhaney (1973) and Darvish (2001).The core-samples were cut indifferently on the two hemispheres using a cylindrical sharp tube. All cylindrical samples were taken in the corona radiata region and contained only white matter to avoid inhomogeneity effects. From the core-samples, 10 and 20 mm-diameter disc-shaped sample were cut using a microtome with vibrating razor blade. The disc-shaped specimen heights varied between 150 µm and 2.25 mm. After the cut, each sample was submerged in Ringer-Lactate solution and preserved at 6°C before the test to slow down the degeneracy of the tissue. Testing was then completed within the day or two days. Two series of experiments were carried out on two different devices one for small strain at height frequency and a second for large strain under relaxation.

The first experimental setup, named "High Frequency Rheometer" (HFR), consisted in a custom-designed oscillatory shear testing device associated with signal generator followed by an amplifier to generate the input signal and with a charge amplifier to observe the output signal. The prescribed translation was applied on the one plate by transmitting piezoelectrical oscillator, while the resulting shear force was measured on the other plate by receiving piezoelectrical oscillator. The imposed displacement was 50 Å and led a maximum strain of the order of microstrain. The frequency-range was from 0.1 Hz to 10000 Hz. A general description of this equipment is illustrated in Figure 3.

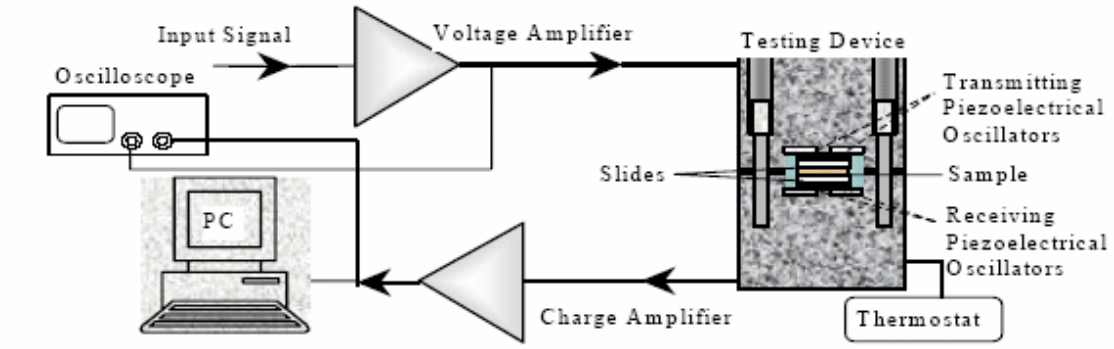

Figure 3 : Diagram of the High Frequency Rheometer measuring equipment.

The High Frequency Rheometer was calibrated by testing solid and fluid materials with known properties. The accuracy was of 94% for the shear modulus of a rubber and it was of 99.9% for the dynamic viscosity of air (at 30°C) between 0.1 and 10000 Hz. The effect of the inertial forces was taking into account during the tests and could be considered negligible under 6000 Hz. Over 6000 Hz, the measured modulus value was random.

Eighteen samples were tested with the HFR device. Samples were glued between the plates of the apparatus to prevent the slipping effect The shear plane was the sagittal plane and the testing temperature was 37°C. The applied strain level of 0.002 % corresponded to the measurement of the linear complex shear modulus. The mean and the standard deviation of the dynamic shear modulus for the porcine white matter from this HFR device is shown on Fig.4 in term of complex shear modulus. Quantitatively, the storage (G') and loss (G") modulus increased significantly as a function of frequency from 2.1 ± 0.9 kPa to 16.8 ± 2.0 kPa and 0.4 ± 0.2 kPa to 18.7 ± 2.3 kPa respectively between 0.1 and 6310 Hz.

Traditionally, the shear linear behaviour of the brain tissue is implemented into the finite element model by the relaxation modulus from a generalised Maxwell model in conformity with equation 2.

$$G(t) = G_e + \sum_{i=1}^{n} G_i e^{-\beta_i t} \qquad (2)$$

where G_e is the long-term shear modulus, G_i and β_i are the shear modulus and the decay constant respectively of the i^{th} mode and t is the duration. These linear material parameters are determined from the experimental relaxation modulus (Fig.4a) and are listed in the Table 2. It was possible, with the identified parameters to fit accurately both dynamic moduli G' and G'' as illustrated in Figure 4b and this is generally not the case in the literature.

In addition a second apparatus, a classical shear rheometer (Bohlin) was used to consolidate the results. The linear shear properties of brain tissue over a large frequency range were obtained from thin brain samples (mean thickness = 400 µm, diameter = 10 mm) tested with the HFR device. The reliability of the current data was checked by testing thicker brain samples (thickness = 2250 µm, diameter = 20 mm) with a standard rheometer (Bohlin C-VOR 150). Samples was tested in relaxation and the results in the linear domain were shown in Figure 4a. A good agreement was found between the two data sets, which confirmed the robustness of the used experimental protocol (slip, dehydration and degeneracy precautions).

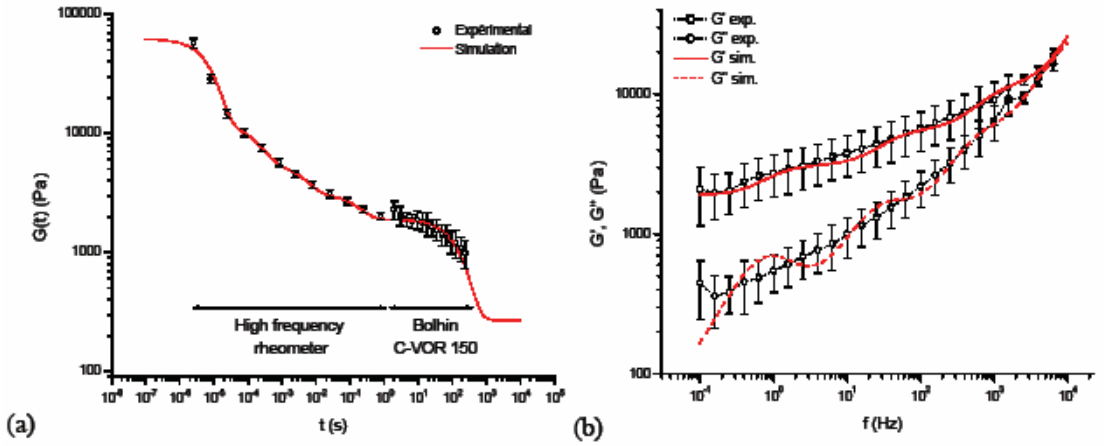

Fig. 4 (a) Experimental data and modelling of the relaxation modulus of the porcine white matter (*corona radiata*) via a linear viscoelastic five-mode-Maxwell model, (b) superimposition of the experimental and simulated G' and G'' evolution in the frequency domain.

The non-linear behaviour of brain material was investigated with the same standard shear rheometer (Bolhin C-VOR 150). Relaxation tests under torsional loading were performed by applying increasing strains from 0.1 to 50% during a transient loading. Although the large strain results were based on few

brain samples, it is interesting to note that they were already in accordance with some results reported in the literature (Darvish 2001; Brands 2000). Nevertheless, the current findings were not statistically valid and should be interpreted as a trend rather than reference data. The results were represented in terms of associated stresses as reported in Figure 5. It is interesting to note that an equilibrium phase appears at the long time for each strain level (Figure 5a) as it can be observed for viscoelastic material. Under incompressible isotropic hypothesis and hysteretic free material behaviour, the rubberlike behaviour of brain material can be modelled by a third order Ogden hyperelastic model (Mendis et al., 1995; Brands et al., 2000; Prange et al., 2000) accordingly to equation 3.

$$\sigma(\lambda, t \to \infty) = \sum_{k}^{3} \mu_k^g \frac{\lambda^{\alpha_k} - \lambda^{-\alpha_k}}{\lambda + \lambda^{-1}} \qquad (3)$$

where λ is the maximum principal stretch ratio and and α are the material properties.

The non-linear material properties used in the finite element model are listed in the Table 3. In order to characterise the incompressibility of the brain tissue, a Poisson ration of 0.499999 is implemented. Figure 5b compares the model's response to the experimental data. The mean accuracy of the Ogden model fit was 73%. However, the model was more accurate over 10% of strain (95%) and less accurate under 10% of strain (36%).

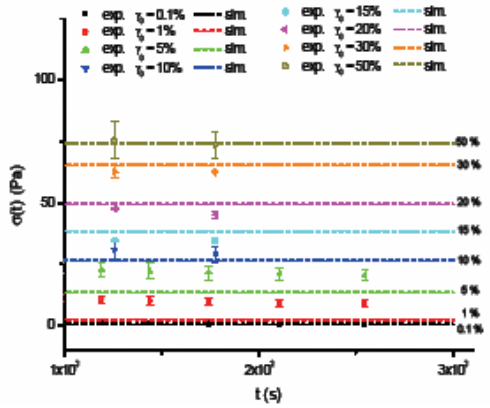

Fig.5 Experimental results and prediction of the Ogden hyperelastic model for the long-term shear stress under large strain conditions.

Results relative to brain investigation are firstly new experimental data for porcine brain. The data in this paper provide new information about the mechanical response of the brain at high frequencies in order to better simulate brain behaviour under short impact. Another reason for this study was to clarify the material characterization of the brain in the linear domain since a great discrepancy in results is to be regretted in the literature. With these intentions, two series of experiments were performed with different sizes of samples and mode of excitation. Piezo rheological tests under translation shearing permitted to obtain real (G') and imaginary (G'') part of the complex shear modulus between 0.1 and about 5000 Hz. These modulli (G') and (G'') increased from 2.1 ± 0.9 kPa to 16.8 ± 2.0 kPa and 0.4 ± 0.2 kPa to 18.7 ± 2.3 kPa respectively between 0.1 and 6310 Hz. In a second approach the non linear brain behaviour were obtained through torsional shearing, for respectively 10, 20 and 50% shearing deformation relaxation moduli of 270, 230 and 150 Pa were obtained. To compare our findings with previous studies on cerebral tissue, an overview of literature data and results of this study is presented in Figure 6.

Two improved brain constitutive laws were finally identified, a linear visco-elastic one, based on a five mode Maxwell model which perfectly reproduces the brain elastic and viscous behaviour up to 5000 Hz and a non linear hyper-elastic Ogden model which reproduces realistically the large strain tests.

It must be mentioned that only white matter has been considered in this study focusing on porcine

brain and not human brain. Further investigation is needed also at the non linear brain behaviour under large deformation level were strain rate must be considered.

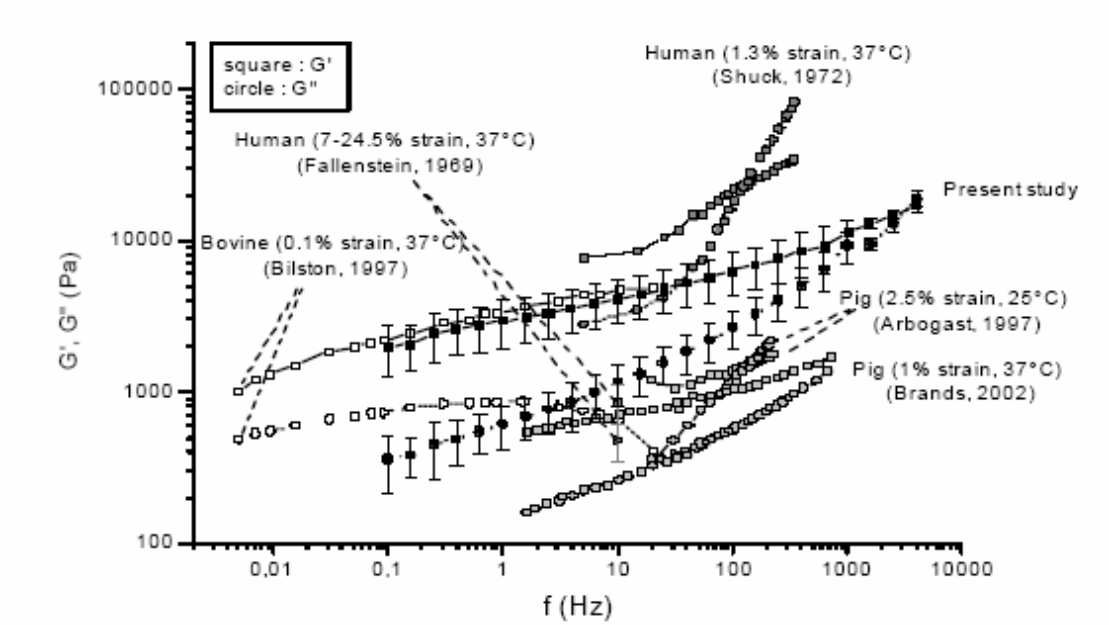

Fig.6 : Complex shear modulus reported in the literature superimposed to the present study results.

4 Model Validation

General aspects : In order to obtain a complete 3D FEM of the human head, the new skull was coupled with the cerebrum, cerebellum, falx, tentorium and the brain stem meshing taken from the ULP model (Willinger et al., 2000). The cerebral-spinal fluid (CSF) was adjusted in order to allow a mesh continuity with the inner table and the brain. Two layers of brick elements in continuity with the outer table model the scalp. Overall, the current head model consists of 79015 nodes and 74243 elements divided in 48266 bricks and 25977 shells.

The material properties of the intra-cerebral membranes, the CSF and the scalp are similar to those used in ULP's model (Willinger et al., 2000). The skull (tables and diploë) was modelled by an elasto-plastic Johnson cook law. The viscoelastic and hyperelastic properties assigned to the brain come from our experimental data.

Skull fracture : In order to validate the new improved skull finite element model to predict a skull fracture in case of very hard impact, two impacts were simulated: a frontal shock and an impact to the vertex reported by Yoganandan et al. in 1994. The numerical results were compared with experimental cadaver test data. However, only results relative to the vertex impact are presented in this paper. The impact configuration is shown in Figure 7a. The surface of the impactor was modelled by a 96 mm diameter rigid sphere. Initial conditions were similar to the experimental ones i.e. a mass of 1.213 kg with an initial speed of 7.1 ms^{-1}. The base of the skull was embedded as in the experience. For the model validation, the contact force and the deflection of the skull at the impact site, were computed. The

numerical force-deflection curves are compared to the average dynamic response of experimental data in Figure 7b. The dynamical model responses agree well with the experimental results, both the fracture force and the stiffness level. The model indicates multiple fracture located around the impact point which complies with pathological observations. We can note that the linear fracture are propagated along the reinforced beam (Spheno-frontal beam) and perpendicular to this for the inner and the outer tables.

Skull fracture modelling is an important safety aspect as far as pedestrian safety is concerned. After the present geometry improvement, further analysis is needed at the bone constitutive laws level specially for the rupture phenomenon by conducing dynamical tests on bone samples. A validation in term of depressive fracture is also needed for further validation.

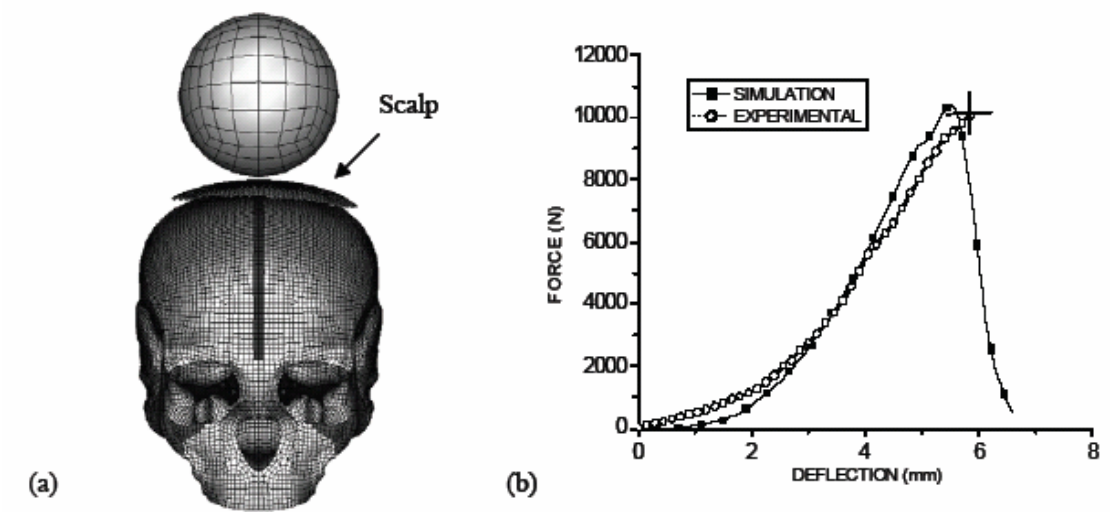

Fig.7 (a)The 3D human head model under vertex impact configuration for Yoganandan's impact simulation (b) experimental vs simulated force deflection curves until fracture.(gives the corridor of Yoganandan's experimental results).

Intracranial behaviour: Validation of intracranial behaviour is obtained against new cadaveric brain motion data recorded by Hardy et al. (2001). Test C755-T2 was chosen for this purpose. It's an occipital impact with an impact velocity about 2 m/s. The peak resultant linear and angular accelerations at the CG of the head were 24 G over a 20 millisecond duration and 1,813 rad/s2,respectively. For this validation the skull is considered as a rigid body. The six components of the acceleration reported in Figure 9 were applied to the center of gravity of the model. Ten nodes in approximately the same position as Hardy's brain experimental targets were identified and their nodal displacement were calculated in the sagittal plane.

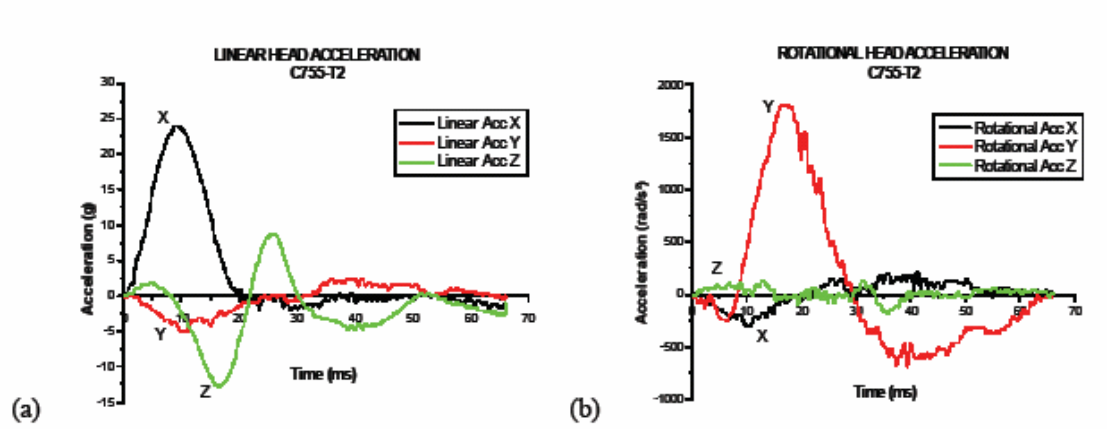

Fig. 8 The six components of the acceleration (Linear (a), rotational (b)) applied at the CG of the model corresponding to the linear and angular acceleration measured at the CG of the head from an occipital impact test C755-T2.

Upon validated in the brain material identification step both new constitutive laws are implemented in a FE code (Radioss Crash) and head model validation in terms of intracerebral deformation is conducted in conformity with Hardy's brain motion recordings impact. Figure 9 shows the models predicted and experimentally obtained target motions for Test C755-T2 for both linear viscoelastic and non-linear hyperelastic brain constitutive laws. The overall brain motion exhibited a looping path with varying degrees of excursion depending of the target location. By comparing the predicted brain motions to experimental data, it appears that the loop are very similar. The brain motion amplitude, with a hyper-elastic law, increase to 5mm whereas this amplitudes is only about 3mm with the visco-elastic brain. It corresponds to an error about 10% for the hyperelastic brain and about 50% for the vicoelastic brain.

Figure 10 shows four NDT targets results in X and Z direction. These curves illustrate a good accordance between simulated and experimental target displacement evolution when the brain is represented by a non-linear hyper-elastic constitutive law. We can note that the viscoelastic model has damping whereas the hyperelastic model has no damping which can explain why the displacement amplitudes were higher in the hyperelastic model. However, we can observe that the directions of motion for the targets a1 and p1 were different to those obtained experimentally especially in Z direction.

Only one occipital shock was investigated in this paper and it should be mentioned that the conducted validation considers 20 millisecond duration impact whereas often shorter impacts are considered for FE model validation. Further investigations are needed at this intracranial behaviour validation by considering also lateral impacts with various impact duration.

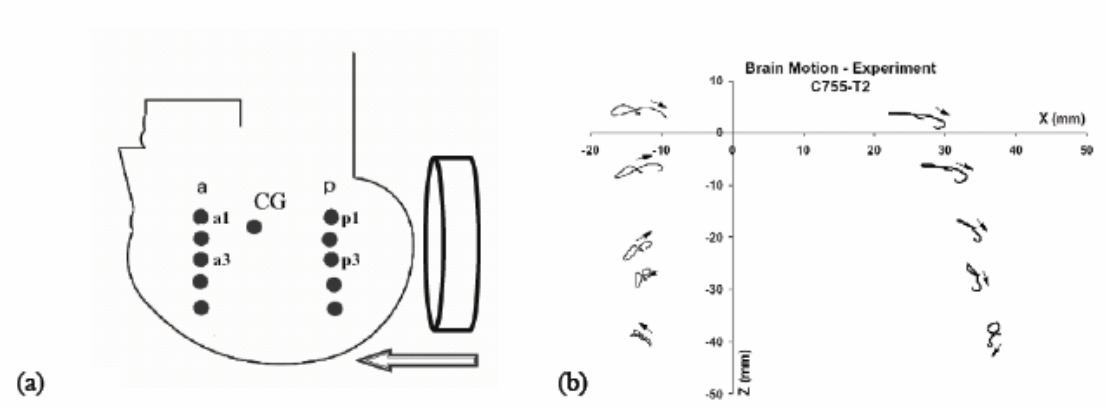

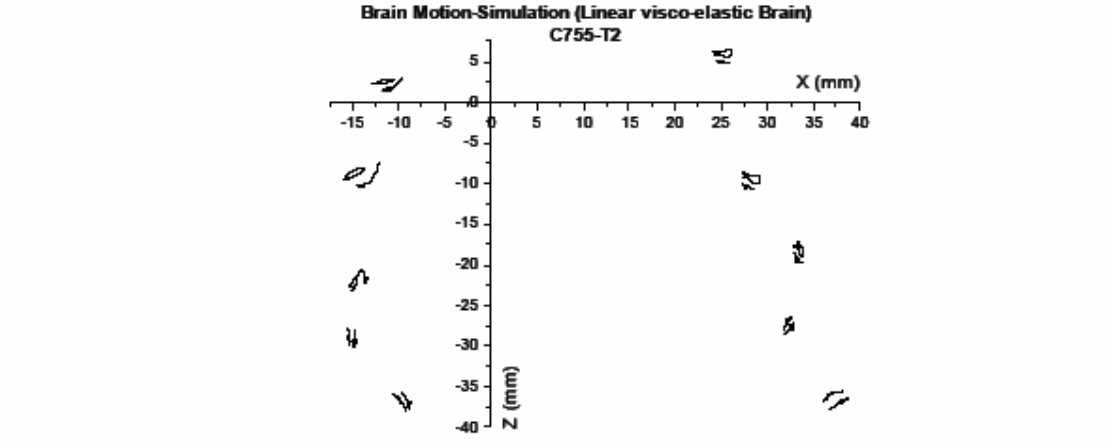

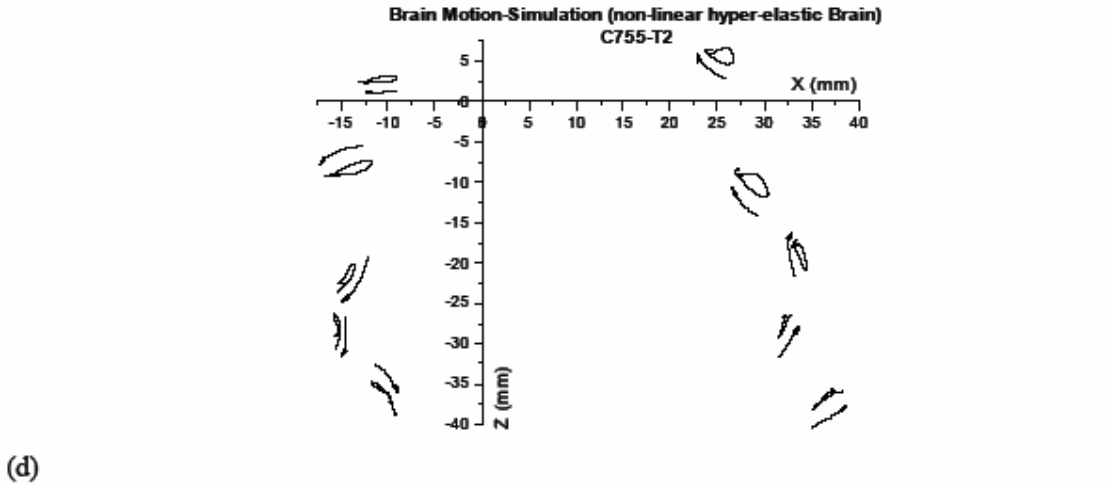

Fig. 9 The orientation of the head, the impactor location and the NDT locations are illustrated in (a). Brain motion at various locations in a sagittal plane during test C755-T2 : (b) Experimental data; (c) Model results with a visco elastic brain; (d) Model results with a hyper-elastic brain. The origin is the center of gravity of the head.

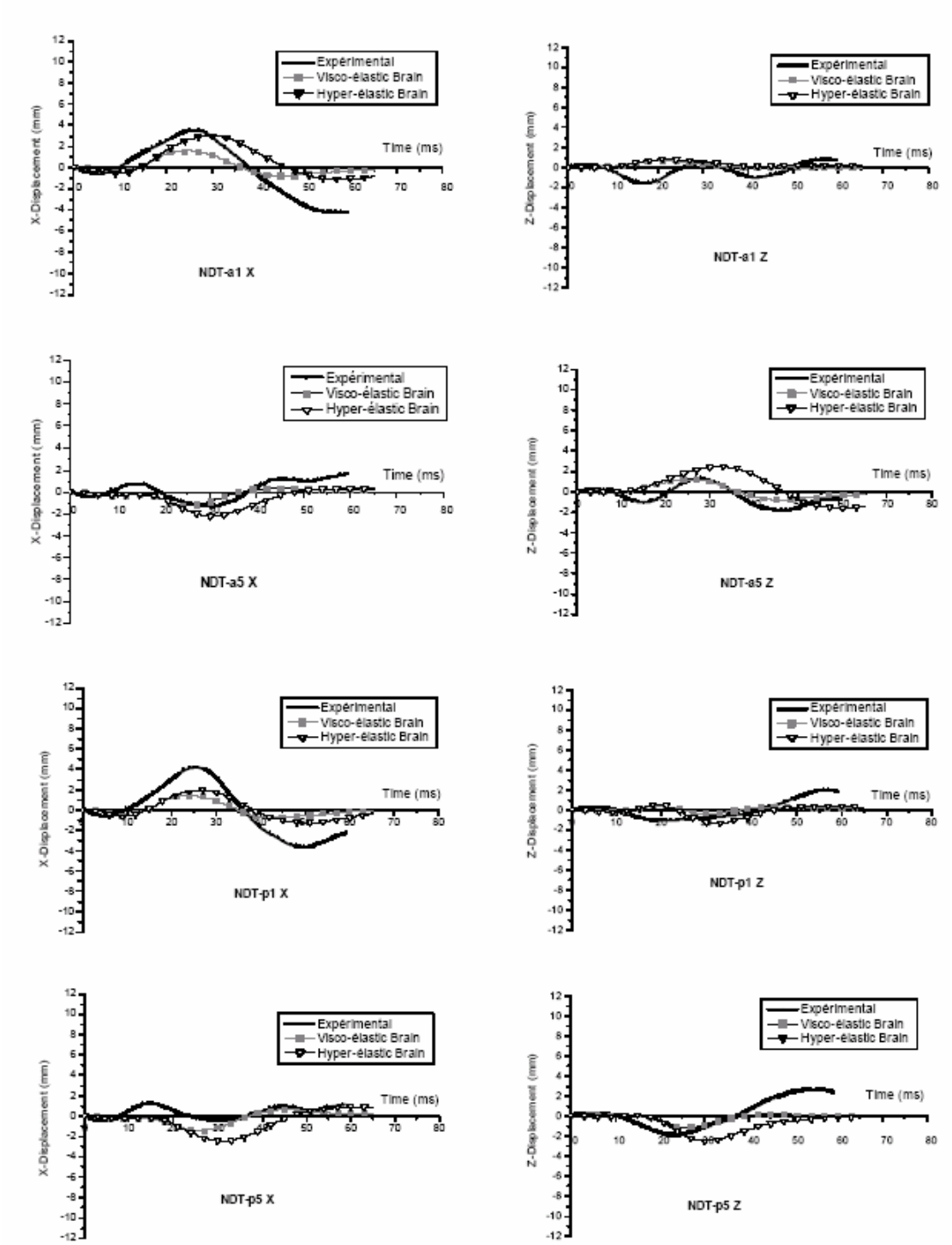

Fig.10 Test C755-T2 displacement-time histories of four neutral density targets measured experimentally (Hardy et al. 2001) and computed with the ULP 2004 head model using two brain's laws (visco-elastic and hyper elastic).

5 Conclusions

The improved skull model is characterized by a refined mesh respecting the skull thickness variation and integrating the skull anatomical reinforcement beams. The detailed skull model includes 25496 shell

elements for the inner and outer table and 16 322 brick elements for the diploë. Elasto-plastic brittle constitutive laws of both bone constituents have been implemented in the model with values from the literature. It was possible to couple this skull with the brain model developed previously at ULP and to simulate linear fractures produced experimentally and reported in the literature.

Original brain investigation are firstly a new set of experimental data for porcine brain at high frequency. Piezo rheological tests permitted to obtain real (G') and imaginary (G'') part of the complex shear modulus between 0.1 and about 6000 Hz. These modulli (G') and (G'') increased from 2.1 ± 0.9 kPa to 16.8 ± 2.0 kPa and 0.4 ± 0.2 kPa to 18.7 ± 2.3 kPa respectively between 0.1 and 6000 Hz. For the non linear brain behaviour, relaxation modulli of 270, 230 and 150 Pa were obtained for respectively 10, 20 and 50% shearing deformation.

Two improved brain constitutive laws were finally identified, a linear visco-elastic one, based on a five mode Maxwell model which perfectly reproduces the brain elastic and viscous behaviour up to 5000 Hz and a non linear hyperelastic Ogden model which reproduces realistically the large strain relaxation tests.

Upon validated against brain characterisation tests both new constitutive laws are implemented in Radioss FE code and head model validation in terms of intra-cerebral deformation is conduced in conformity with Hardy's in vitro brain motion recordings under head impact. The applied impact is characterized by a 25 G's skull acceleration over a 20 millisecond duration approximately. Recorded brain amplitude motion lies in a 5 to 6 mm range. When new proposed brain constitutive laws are used, brain motion amplitudes increase from 3 mm with the visco-elastic linear model to 5 mm with the non linear hyperelastic model.

This conclusion shows that both high frequency data and large strain must be considered in order to enlarge head FE model application field. Indeed validation of models under a large range of impacts is needed before the next investigation step which is real world accident simulation and injury criteria definition.

6 References

1. Arbogast, K.B. & Margulies, S.S., Regional differences in mechanical properties of the porcine central nervous system. Proc. Of Car Crash Conf., SAE 973336, 1997, pp. 293-300.
2. Bilston LE, Liu Z, Phan-Thien N., Linear viscoelastic properties of bovine brain tissue in shear. Biorheology 1997, 34, pp.377-385.
3. Bilston, L.E., Liu, Z., Phan-Thien, N., Large strain behaviour of brain tissue in shear: some new experimental data and differential constitutive model. Biorheology 38(4), 2001, pp.335-345.
4. Brands, D.W.A., Bovendeerd, P.H., Peters, G.W.M., Finite shear behaviour of brain tissue under impact loading. ASME-WAM, Conf. on Crashworthiness, Occupant Protection and Biomechanics in Transportation Systems, AMD-Vol. 246/BED-49, 2000, pp.175-188.
5. Brands, D.W., Predicting Brain Mechanics During Closed Head Impact – Numerical and Constitutive Aspects. Ph.D. dissertation, University of Eindhoven, The Netherlands, 2002.
6. Brands DWA, Bovendeerd PH, Wismans JSHM., On the Potential Importance of Non-Linear Viscoelastic Material Modelling for Numerical Prediction of Brain Tissue Response. Stapp Car Crash Journal., Vol 46, 2002, pp.103-121.
7. Christensen, R.M., Theory of viscoelasticity. 2nd éd., Academic Press, New-York, 1982.
8. Darvish, K.K., Crandall, J.R., Nonlinear viscoelastic effects in oscillatory shear deformation of brain tissue. Medical Engineering & Physics 23, 2001, pp.633-645.
9. Donnelly, B., Medige, J., Shear properties of human brain tissue. Journal of Biomechanical Engineering 119, 1997, pp.423-432.
10. Fallenstein, G.T. & Hulce, V.D., Dynamic mechanical properties of human brain tissue. J of Biomechanics, 2, 1969, pp. 217-226.
11. Hardy W.N., Foster, C.D., Mason, M.J., Yang, K.H., King, A.I., and Tashman, S., Investigation of head injury mechanisms using neutral density technology and high-speed biplanar X-ray. Stapp Car Crash Journal, 2001, pp.375.
12. Hickling, R., Wenner, M.L., Mathematical model of a head subjected to an axisymmetric impact. Journal of Biomechanics 6, 1973, pp.115-132.

13. Kamina P., Précis d'anatomie clinique, Tome II, Editions Maloine, 2002.
14. Kang H.S., Willinger R., Diaw B., Chinn B., Validation of a 3D anatomic human head model and replication of head impact in motorcycle accident by finite element modeling, Proc. of the 41th Stapp Car Crash Conf, 1997, pp. 329-338.
15. King A., Yang K., Zhang L., Hardy W., Is head injury caused by linear or angular acceleration?, Proc. of the IRCOBI Conf. 2003, 2003, pp. 1-12.
16. Kleiven S., Hardy W., Correlation of an FE model of the human head with local brain motion-Consequences for injury prediction, Proc. of the 46th Stapp Car Crash Conf., 2002, pp. 123-144.
17. McElhaney, J.H., Roberts, V.L. & Hilyard, J.F., Handbook of Human Tolerance. Japan Automobile Research Institut, Inc., 1976, pp. 143.
18. McElhaney, J.H., Melvin, J.W., Roberts, V.L., Portnoy, H.D., Dynamic characteristics of the tissues of the head. In: Perspectives in Biomedical Engineering, ed. R.M. Kenedi, Macmillian Press Ltd., London, 1973, pp.215-222.
19. Mendis, K.K., Stalnaker, R.L., Advani, S.H., A constitutive relationship for large deformation finite element modeling of brain tissue. Journal of Biomechanical Engineering 117, 1995, pp. 279-285.
20. Peters, G.W.M., Meulman, J.H., Sauren, A.A.H.J., The applicability of the time/temperature superposition principle to the brain tissue. Biorheology 34(2), 1997, pp. 127-138.
21. Prange, M.T., Meaney, D.F., S.S., Margulies, Defining brain mechanical properties: effects of region, direction and species. Proc. Of the 44th Stapp Car Crash Conf., 2000-01-SC15, 2000, pp.205-213.
22. Shuck, L.Z. & Advani S.H., Rheological response of human brain tissue in shear. J of Basic Engineering: 23. Transactions of the ASME, 1972, pp. 905-911.
23. Stalnaker RL. Mechanical properties of the head. Ph.D. Dissertation Thesis, West Virginia University, Morgantown, WV, USA, 1969.
24. Takhounts E., Eppinger R., On the development of the SIMon finite element head model, Proc. Of the 47th Stapp Car Crash Conf., 2003, 107-133.
25. Thibault L; E., Gennarelli T.A., Margulies S.S., Marcus J., Eppinger R., The strain dependant pathophysiological consequences of inertial loading on central nervous system tissue, Proc. of the IRCOBI Conf, 1990 pp. 191-202.
26. Willinger R., Baumgartner D., Human head tolerance limits to specific injury mechanisms, International journal of Crashworthiness, Vol 8, No 6, 2003, pp.605-617.
27. Willinger R., Baumgartner D., Chinn B., Neale M., Head tolerance limits derived from numerical replication of real world accidents, Proc. of the IRCOBI Conf. 2000, 2000, pp. 209-222.
28. Wood J.L., Dynamical Response of Human Cranial Bone, J. Biomech. 4, 1971, pp.1-12.
29. Yoganandan N. - Biomechanics of Skull Fracture, Proceed. of Head Injury 94 Symposium, Washington DC, 1994.
30. Zhang L., King KH., Dwarampudi R., Omori K., Li TB., Hardy W., Khalil T., King AI., Recent Advances in Brain Injury Research: A New Human Head Model Development and Validation, Stapp Car Crash Journal, Vol 45, 2001, pp. –375.